Year: 2020

Ultrafast Intracranial Vessel Imaging With Non-Cartesian Spiral 3-Dimensional Time-of-Flight Magnetic Resonance Angiography at 1.5 T: An In Vitro and Clinical Study in Healthy Volunteers

Sartoretti, Thomas ; van Smoorenburg, Luuk ; Sartoretti, Elisabeth ; Schwenk, Árpád ; Binkert, Christoph A ; Kulcsár, Zsolt ; Becker, Anton S ; Graf, Nicole ; Wyss, Michael ; Sartoretti-Schefer, Sabine

Abstract: OBJECTIVES Non-Cartesian spiral magnetic resonance (MR) acquisition may enable higher scan speeds, as the spiral traverses the k-space more efficiently per given time than in Cartesian trajectories. Spiral MR imaging can be implemented in time-of-flight (TOF) MR angiography (MRA) sequences. In this study, we tested the performance of five 3-dimensional TOF MRA sequences for intracranial vessel imaging at 1.5 T with qualitative and quantitative image quality metrics based on in vitro and in vivo measurements. Specifically, 3 novel spiral TOF MRA sequences (spiral-TOFs) and a compressed sensing (CS) technology-accelerated TOF MRA sequence (CS 3.5) were compared with a conventional (criterion standard) parallel imaging-accelerated TOF MRA sequence (SENSE). MATERIALS AND METHODS The SENSE sequence (5:08 minutes) was compared with the CS 3.5 sequence (3:06 minutes) and a spiral-TOF (spiral, 1:32 minutes), all with identical resolutions. In addition, 2 further isotropic spiral-TOFs (spiral 0.8, 2:12 minutes; spiral 0.6, 5:22 minutes) with higher resolution were compared with the SENSE. First, vessel tracking experiments were performed in vitro with a dedicated vascular phantom to determine possible differences in the depiction of cross-sectional areas of vessel segments. For the in vitro tests, an additional 3-dimensional proton density-weighted sequence was added for comparison reasons. Second, 3 readers blinded to sequence details assessed qualitative (16 features) and 2 readers assessed quantitative (contrast-to-noise ratio [CNR], contrast ratio [CR], vessel sharpness, and full width at half maximum edge criterion measurements) image quality based on images acquired from scanning 10 healthy volunteers with all 5 TOF sequences. Scores from quantitative image quality analysis were compared with Kruskal-Wallis, analysis of variance, or Welch's analysis of variance, followed by Dunnett's or Dunnett's T3 post hoc tests. Scores from qualitative image quality analysis were compared with exact binomial tests, and the level of interreader agreement was determined with Krippendorff's alpha. RESULTS Concerning the in vitro tests, there were no significant differences between the 5 TOFs and the proton density-weighted sequence in measuring cross-sectional areas of vessel segments ($P = 0.904$). As for the in vivo tests, the CS 3.5 exhibited equal qualitative image quality as the SENSE, whereas the 3 spiral-TOFs outperformed the SENSE in several categories (P values from 0.002 to 0.031). Specifically, the spiral 0.8 and 0.6 sequences achieved significantly higher scores in 12 categories. Interreader agreement ranged from poor (alpha = -0.013, visualization of internal carotid artery segment C7) to substantial (alpha = 0.737, number of vessels visible, sagittal). As for the quantitative metrics, the CS 3.5 and all 3 spiral-TOFs presented with significantly worse CNR than the SENSE ([mean ± SD] SENSE 37.48 ± 7.13 vs CS 3.5 31.14 ± 5.97 vs spiral 19.77 ± 1.65 vs spiral 0.8 16.18 ± 2.14 vs spiral 0.6 10.37 ± 1.05). The CR values did not differ significantly between the SENSE and the other TOFs except for the spiral sequence that showed significantly improved CR (SENSE 0.53 ± 0.03 vs spiral 0.56 ± 0.03). As for vessel sharpness, the SENSE was outperformed by all spiral-TOFs (SENSE 0.37 ± 0.03 vs spiral 0.52 ± 0.07 vs spiral 0.8 0.53 ± 0.08 vs spiral 0.6 0.73 ± 0.09), whereas the CS 3.5 performed equally well (SENSE 0.37 ± 0.03 vs CS 3.5 0.37 ± 0.03). Full width at half maximum values did not differ significantly between any TOF. CONCLUSIONS Spiral-TOFs may deliver high-quality intracranial vessel

imaging thus matching the performance of conventional parallel imaging-accelerated TOFs (such as the SENSE). Specifically, imaging can be performed at unprecedented scan times as short as 1:32 minutes per sequence (70.12% scan time reduction compared with SENSE). Optionally, spiral imaging may also be used to increase spatial resolution while maintaining the scan time of a Cartesian-based acquisition schema. The CNR was decreased in spiral-TOF images.

DOI: https://doi.org/10.1097/RLI.0000000000000641

Ultrafast Intracranial Vessel Imaging With Non-Cartesian Spiral 3-Dimensional Time-of-Flight Magnetic Resonance Angiography at 1.5 T

An In Vitro and Clinical Study in Healthy Volunteers

Thomas Sartoretti, Luuk van Smoorenburg, BSc,* Elisabeth Sartoretti,* Árpád Schwenk, MD,* Christoph A. Binkert, MD,* Zsolt Kulcsár, MD, PhD,† Anton S. Becker, MD, PhD,‡§ Nicole Graf, PhD,|| Michael Wyss, BSc,*¶ and Sabine Sartoretti-Schefer, MD**

Objectives: Non-Cartesian spiral magnetic resonance (MR) acquisition may enable higher scan speeds, as the spiral traverses the k-space more efficiently per given time than in Cartesian trajectories. Spiral MR imaging can be implemented in time-of-flight (TOF) MR angiography (MRA) sequences. In this study, we tested the performance of five 3-dimensional TOF MRA sequences for intracranial vessel imaging at 1.5 T with qualitative and quantitative image quality metrics based on in vitro and in vivo measurements. Specifically, 3 novel spiral TOF MRA sequences (spiral-TOFs) and a compressed sensing (CS) technology–accelerated TOF MRA sequence (CS 3.5) were compared with a conventional (criterion standard) parallel imaging–accelerated TOF MRA sequence (SENSE).

Materials and Methods: The SENSE sequence (5:08 minutes) was compared with the CS 3.5 sequence (3:06 minutes) and a spiral-TOF (spiral, 1:32 minutes), all with identical resolutions. In addition, 2 further isotropic spiral-TOFs (spiral 0.8, 2:12 minutes; spiral 0.6, 5:22 minutes) with higher resolution were compared with the SENSE. First, vessel tracking experiments were performed in vitro with a dedicated vascular phantom to determine possible differences in the depiction of cross-sectional areas of vessel segments. For the in vitro tests, an additional 3-dimensional proton density-weighted sequence was added for comparison reasons. Second, 3 readers blinded to sequence details assessed qualitative (16 features) and 2 readers assessed quantitative (contrast-to-noise ratio [CNR], contrast ratio [CR], vessel sharpness, and full width at half maximum edge criterion measurements) image quality based on images acquired from scanning 10 healthy volunteers with all 5 TOF sequences. Scores from quantitative image quality analysis were compared with Kruskal-Wallis, analysis of variance, or Welch's analysis of variance, followed by Dunnett's or Dunnett's T3 post hoc tests. Scores from qualitative image quality analysis were compared with exact binomial tests, and the level of interreader agreement was determined with Krippendorff's alpha.

Results: Concerning the in vitro tests, there were no significant differences between the 5 TOFs and the proton density-weighted sequence in measuring cross-sectional areas of vessel segments ($P = 0.904$). As for the in vivo tests, the CS 3.5 exhibited equal qualitative image quality as the SENSE, whereas the 3 spiral-TOFs outperformed the SENSE in several categories (P values from 0.002 to 0.031). Specifically, the spiral 0.8 and 0.6 sequences achieved significantly higher scores in 12 categories. Interreader agreement ranged from poor (alpha = −0.013, visualization of internal carotid artery segment C7) to substantial (alpha = 0.737, number of vessels visible, sagittal). As for the quantitative metrics, the CS 3.5 and all 3 spiral-TOFs presented with significantly worse CNR than the SENSE ([mean ± SD] SENSE 37.48 ± 7.13 vs CS 3.5 31.14 ± 5.97 vs spiral 19.77 ± 1.65 vs spiral 0.8 16.18 ± 2.14 vs spiral 0.6 10.37 ± 1.05). The CR values did not differ significantly between the SENSE and the other TOFs except for the spiral sequence that showed significantly improved CR (SENSE 0.53 ± 0.03 vs spiral 0.56 ± 0.03). As for vessel sharpness, the SENSE was outperformed by all spiral-TOFs (SENSE 0.37 ± 0.03 vs spiral 0.52 ± 0.07 vs spiral 0.8 0.53 ± 0.08 vs spiral 0.6 0.73 ± 0.09), whereas the CS 3.5 performed equally well (SENSE 0.37 ± 0.03 vs CS 3.5 0.37 ± 0.03). Full width at half maximum values did not differ significantly between any TOF.

Conclusions: Spiral-TOFs may deliver high-quality intracranial vessel imaging thus matching the performance of conventional parallel imaging–accelerated TOFs (such as the SENSE). Specifically, imaging can be performed at unprecedented scan times as short as 1:32 minutes per sequence (70.12% scan time reduction compared with SENSE). Optionally, spiral imaging may also be used to increase spatial resolution while maintaining the scan time of a Cartesian-based acquisition schema. The CNR was decreased in spiral-TOF images.

Key Words: spiral, sparse undersampling, compressed sensing, magnetic resonance angiography, time of flight

(*Invest Radiol* 2019;00: 00–00)

Time-of-flight (TOF) magnetic resonance angiography (MRA) is a noninvasive and contrast media–free MR technique that can be used to image intracranial vessels. Time-of-flight MRA has been shown to be an effective and reliable alternative to digital subtraction angiography and has thus been widely adopted in clinical institutions for use in patients with suspected intracranial vascular disorders such as stenoses or aneurysms.[1–7]

Currently, parallel imaging (PI; ie, techniques such as sensitivity encoding, SENSE)–accelerated TOF MRA sequences are considered the criterion standard for intracranial vessel MR imaging.[8–10] Parallel imaging is a common k-space undersampling method that relies on the reduction of the number of phase-encoding steps. The acceleration factor chosen for PI imaging, however, rarely exceeds 2 or 3, and thus PI-accelerated TOFs are still quite time-consuming, thereby rarely achieving scan times below 5 minutes.[2] By combining TOF MRA sequences with compressed sensing (CS) technology, a further reduction of scan times is possible. Compressed sensing algorithms achieve higher k-space undersampling by using the underlying sparsity in an appropriate transform domain.[1–7]

Recent studies demonstrating the efficacy of CS-accelerated TOFs have employed a range of sequences of which some even achieve scan times of slightly above 2:30 minutes.[1,2,6,7] Although this represents a considerable time saving in comparison to conventional PI-accelerated TOFs, a

Received for publication October 2, 2019; and accepted for publication, after revision, October 25, 2019.

From the *Institute of Radiology, Kantonsspital Winterthur, Winterthur; †Department of Neuroradiology, and ‡Institute of Diagnostic and Interventional Radiology, University Hospital Zürich, University of Zürich, Zürich, Switzerland; §Department of Radiology, Memorial Sloan Kettering Cancer Center, New York, NY; || Graf Biostatistics, Winterthur; and ¶Philips Healthsystems, Zürich, Switzerland.

Conflicts of interest and source of funding: Michael Wyss is a part-time employee of Philips Healthcare Switzerland. The remaining authors declare that the research was conducted in the absence of any commercial or financial relationships that could be construed as a potential conflict of interest. No funding was received for this study.

Thomas Sartoretti and Luuk van Smoorenburg contributed equally.

Correspondence to: Sabine Sartoretti-Schefer, MD, Institute of Radiology, Kantonsspital Winterthur, Brauerstrasse 15, 8401 Winterthur. E-mail: sabine.sartoretti@ksw.ch.

ISSN: 0020-9996/19/0000–0000

DOI: 10.1097/RLI.0000000000000641

further reduction of scan times considerably below 2 minutes with acceptable image quality seems improbable with the currently available acceleration techniques.

However, spiral MR imaging using a non-Cartesian acquisition technique may enable higher scan speeds, as the spiral traverses the k-space more efficiently per given time than in Cartesian trajectories.[11–15] Although the theoretical concept of spiral MR imaging has been described a long time ago, it has only very recently become a potentially viable option for intracranial vessel imaging with TOF MRA sequences.[11–15]

In this pilot study, we therefore report about the first time use of spiral TOF MRA sequences (spiral-TOF) at 1.5 T for intracranial vessel imaging. To this extent, 3 spiral-TOFs and a CS-accelerated TOF (named CS 3.5) were tested in in vitro experiments with a dedicated intracranial vascular phantom model followed by in vivo imaging in volunteers thus highlighting the spiral-TOFs' and the CS 3.5's performance in comparison to a conventional PI-accelerated TOF sequence (named SENSE) utilizing qualitative and quantitative image quality metrics.

MATERIALS AND METHODS

This study was approved by the Cantonal Ethical Committee Zurich, Zurich, Switzerland (BASEC Number 2018-01275) with written informed consent from all volunteers.

Study Design

In this study, 3 spiral-TOFs and a CS-accelerated TOF (CS 3.5) were evaluated and compared with a PI-accelerated TOF (SENSE, criterion standard) sequence. In the in vitro experiments, the accuracy of the sequences in displaying the cross-sectional area of vessels was assessed with a vascular phantom model[16,17] and a vessel tracking software. In the in vivo part, the 5 sequences were scanned in 10 healthy volunteers thus enabling an intraindividual comparison between the different TOFs. Qualitative image quality was rated in a blinded fashion by 3 readers with a 5-point Likert scale in comparison to the SENSE, and images were quantitatively evaluated by means of contrast-to-noise ratio (CNR), contrast ratio (CR), vessel sharpness (VS), and full width at half maximum edge criterion measurements by 2 readers.

MR Imaging

All images were acquired on a 1.5-T scanner (Ingenia; Philips Healthcare, Best, the Netherlands) using a 16-channel head coil and product software (R5.6). A sagittal 3-dimensional (3D) T1w turbo field echo sequence (field of view, 240 × 240 cm^2; matrix, 240 × 240; number of slices, 275; TR/TE/TI, 7.6/3.5/1000 milliseconds; flip angle, 8 degrees; scan duration, 3 minutes 50 seconds) was used for the planning of the TOFs. The 5 sequences were acquired in identical orientation parallel to the splenium and genu of the corpus callosum (in case of the volunteer scans). All TOFs were based on a multichunk (5 chunks) acquisition and a TONE ramp of 17 degrees at the entry slice, 20 degrees at mid-slab, and 23 degrees near the exiting slice. All TOFs used in this study represent 3D TOF MRA sequences.

Three sequences had an identical geometric resolution (voxel size, 0.82 × 0.82 × 1.2 mm^3): first, the SENSE sequence using the SENSE PI technique (SENSE factor 2, scan duration, 5:08 minutes); second, the CS 3.5 sequence using the compressed SENSE acceleration technique with a variable density Poisson disk-sampling scheme followed by iterative reconstruction (compressed SENSE factor, 3.5; scan duration, 3:06 minutes)[18–20]; and third, a spiral-TOF (abbreviated spiral) based on a stack of spirals with an in-plane spiral-out readout scheme (spiral interleaves, 27; spiral acquisition window, 10 milliseconds; scan duration, 1:32 minutes). In addition, 2 sequences with the same spiral-out readout scheme but higher resolution were acquired—the isotropic spiral-TOF 0.8 (abbreviated spiral 0.8) (voxel size, 0.80 × 0.80 × 0.80 mm^3; scan duration, 2:12 minutes) and the isotropic spiral-TOF 0.6 (abbreviated spiral 0.6) sequences (voxel size, 0.60 × 0.60 × 0.60 mm^3; scan duration, 5:22 minutes). Details of the imaging parameters of all 5 TOFs are given in Table 1, and a diagram of the spiral acquisition method is given in Figure 1. The sequences' parameters were defined based on the vendor's implementation. Specifically, the spiral sequence was provided (and recommended) as such by the vendor and represents a sequence that was optimized by the vendor in terms of performance in the preclinical phase of development. As for the resolutions of the spiral 0.8 and spiral 0.6 sequences, we first chose an isotropic resolution that was as close to the spiral, SENSE, and CS 3.5 sequences resolutions (thus 0.8 mm^3 for the spiral 0.8), and second, the highest possible

TABLE 1. Sequence Parameters of the 3D PDw and TOF MRA Sequences

	3D PDw	SENSE	CS 3.5	Spiral	Spiral 0.8	Spiral 0.6
Field of view, mm	200 × 200 × 90	200 × 200 × 90	200 × 200 × 90	200 × 200 × 90	200 × 200 × 90	200 × 200 × 92
Acq. voxel size, mm	0.5 × 0.5 × 0.5	0.82 × 0.82 × 1.2	0.82 × 0.82 × 1.2	0.82 × 0.82 × 1.2	0.82 × 0.82 × 0.82	0.60 × 0.60 × 0.60
Rec. voxel size, mm	0.5 × 0.5 × 0.5	0.39 × 0.39 × 0.6	0.39 × 0.39 × 0.6	0.39 × 0.39 × 0.6	0.39 × 0.39 × 0.41	0.39 × 0.39 × 0.30
No. slices	180	150	150	150	220	305
TR/TE, ms	1100/32	23/6.9	23/6.9	23/2.3	23/2.3	23/2.3
Flip angle, degree	90	20	20	20	20	20
SENSE factor	NA	2	NA	NA	NA	NA
C-SENSE factor	NA	NA	3.5	NA	NA	NA
Spiral acquisition window/no. spiral interleaves	NA	NA	NA	10 ms/27	10 ms/27	10 ms/48
Saturation slab	0	1	1	1	1	1
Receiver bandwith	440.1 Hz/pixel	108 Hz/pixel	108 Hz/pixel	100 Hz/pixel	100 Hz/pixel	100 Hz/pixel
No. signal averages	1	1	1	1	1	1
Flow compensation	No	Yes	Yes	Yes	Yes	Yes
TONE ramp pulse	NA	Yes	Yes	Yes	Yes	Yes
No. chunks	NA	5	5	5	5	5
Scan duration, min:s	13:09	05:08	03:06	01:32	02:12	05:22

3D indicates 3-dimensional; PDw, proton density-weighted; TOF, time-of-flight; MRA, magnetic resonance angiography.

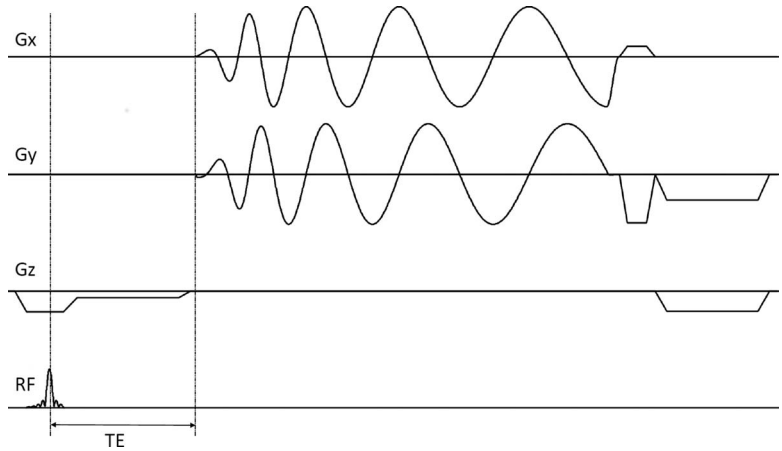

FIGURE 1. Pulse sequence diagram of the spiral-TOF sequences. One in-plane spiral-out trajectory from the whole stack of spirals is shown.

isotropic resolution that was the most comparable in scan time to the SENSE's scan time (thus 0.6 mm^3 for the spiral 0.6). Blurring due to off-resonance was corrected during reconstruction based on a magnetic field map acquired before the spiral scan.

In Vitro Study

In this part of the study, vessel tracking experiments (Fig. 2) were performed with a dedicated vascular phantom model.[16,17] The cross-sectional area of segments of arteries were measured on the maximum intensity projection (MIP) images of the 5 different TOFs and a 3D proton density-weighted (PDw) sequence by the help of a vessel tracking tool called "advanced vessel analysis" AVA on IntelliSpace Portal version 10 (Philips Healthcare, Best, the Netherlands). Cross-sectional area values from the 6 sequences were then compared.

The 3D PDw sequence (isotropic resolution of 0.5 mm^3, Table 1) was added to the in vitro protocol, as it also enables vessel imaging but relies on a different physical principle for image acquisition. Most importantly, however, PDw imaging has previously been described to enable a very accurate depiction of vessels in an in vitro setting,[21] thus making it a good candidate for an additional comparison of cross-sectional areas.

To test this, a self-made model consisting of a plastic box filled with 3 different water-loaded flexible tubes with exactly known dimensions

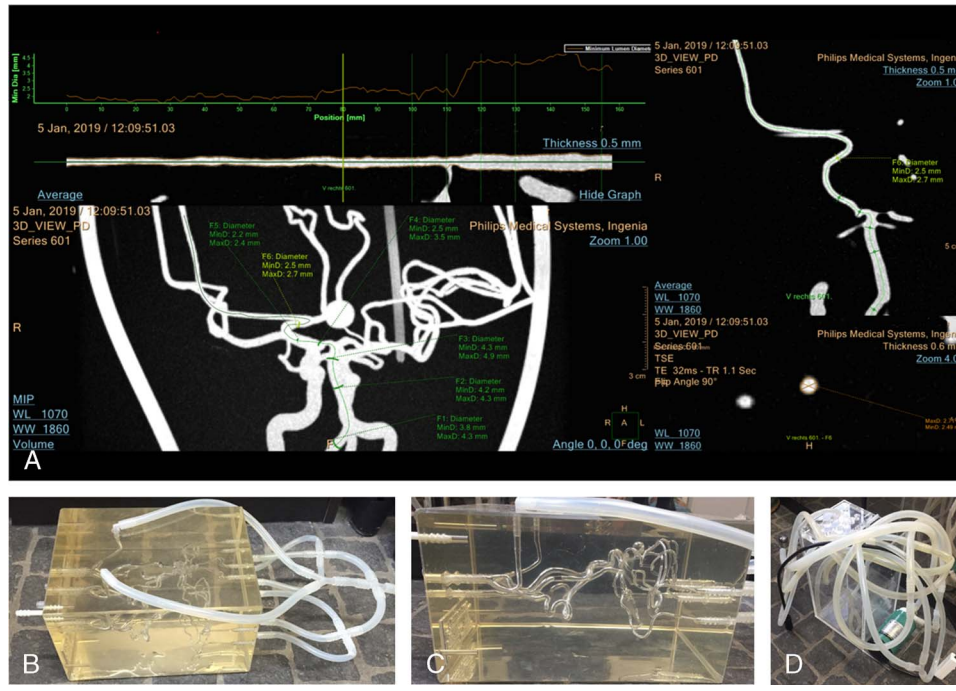

FIGURE 2. In vitro vessel tracking experiments. A, Image depicts a representative example of a vessel tracking experiment performed on the vertebral artery of the dedicated vascular phantom model. The starting point was set at the lowest possible point on the image (which corresponded to 155 mm according to the software's internal reference position system) and 5 further points (thus 6 points in total) were then defined at certain distances away from which cross-sectional area measurements were to be taken (0, 25, 35, 45, 55, 75 [endpoint] mm away from the start point). Cross-sectional areas were calculated based on the average value of the maximum and minimum diameter as seen on (A) in the bottom right corner. B and C, Images show the vascular phantom model. D, Image of the pump that generated a constant water flow through the models vasculature.

(cross-sectional areas of the tubes: [1] 3.142 mm^2, [2] 12.566 mm^2, and [3] 28.274 mm^2) molded into solid agar was scanned with the 3D PDw sequence. Time-of-flight imaging could not be performed with this model as no pump (that could have generated water flow) could be attached to the tubes.

Using the vessel tracking tool, the tubes were tracked on their full length on the PDw images and their dimensions were measured. We determined that the PDw sequence could accurately depict the tubes cross-sectional areas as only small deviations were observed (maximum deviations for each tube: 3% for tube [3] and 5% for tubes [1, 2]). Thus for the in vitro experiments, measurements from the 5 TOF sequences were also compared with the values of the 3D PDw sequence.

As an alternative to the PDw sequence, images from a CT scan could have also functioned as an interesting additional candidate for comparison of measurements. However, this would have required moving the phantom between 2 different scanners, thus requiring realignment of images later in the experiment (for selection of the points used for measurements). Although the CT scan may have theoretically rendered an even more accurate depiction of vessels than the PDw sequence, the realignment process would probably have contributed to a considerable loss of accuracy for.

In a second step, all further in vitro experiments were performed with a dedicated vascular phantom model of intracranial vessels manufactured by Elastrat Sàrl, Geneva, Switzerland (model: H+N-R-A-002).[16,17] Specifically, the model encompasses the circle of Willis with 2 large posterior communicating arteries and 2 small P1 segments of the cerebral posterior artery as well as a large anterior communicating artery (ACA) with a large A1 segment of the anterior cerebral artery on the right side. In addition, an aneurysm is located at the junction of the right A1 segment and the ACA. The phantom was placed into the MR scanner, and a pump, generating a static rather than an oscillating water flow through the vessels of the phantom, was attached.

The phantom was first scanned with the 3D PDw sequence followed by the 5 other sequences (SENSE, CS 3.5, spiral, spiral 0.8, spiral 0.6). During the acquisition of the 3D PDw sequence, the flow pump was switched off, since this image contrast should not be disturbed by flow effects. For the 5 TOF sequences, a constant flow of 7 mL/s at the level of the internal carotid artery (ICA) was pumped through the vascular phantom. The phantom was not moved in between scans thus allowing for the acquisition of 6 geometrically identical image datasets.

Using the vessel tracking tool, the cross-sectional areas of the vessels were then obtained. The tool requires the user to set a start and end point on the vessel that is to be tracked. As a starting point, we selected the lowest possible point on the vertebral artery that was visible on the images. The end point, being 75 mm away from the start point, was set on the P3 segment of the posterior cerebral artery shortly before the end of the vessel within the phantom. Beginning at the start point, 6 points at certain distances afar were defined (ie, 0, 25, 35, 45, 55, 75 mm away from the start point) at which measurements of the vessels cross-sectional area were to be taken. These 6 points corresponded to 1 measurement on the vertebral artery, 2 measurements on the basilar artery, and 1 measurement each of the P1, P2, and P3 segments of the posterior cerebral artery.

A similar procedure was performed for the ICA. The start point was chosen as the lowest possible point on the ICA. The end point was selected 150 mm away from the start point thus being in the M4 segment of the middle cerebral artery. Seven points beginning from the start point were then selected for cross-sectional area measurements, at 0, 30, 60, 90, 120, and 150 (endpoint) mm away from the start point. These 7 points corresponded to 1 measurement in the C1 and 1 measurement in the C3 segments of the ICA and 1 measurement each in the M1, M2, M3, and M4 segments of the middle cerebral artery.

As the phantom was not moved between acquisitions of the different sequences, this process enabled us to always select the exact same points for measurements in all 6 sequences thus explaining the utility of the in vitro tests. The placement of points was performed by a senior neuroradiologist with 30 years of experience (S.S.) and was checked by a second reader with 3 years of experience in medical imaging research (T.S.).

In Vivo Study

Ten healthy volunteers (mean age, 37 ± 14 years; age range, 20–60, 3 women) were recruited. Inclusion criteria for the subjects were older than 18 years, no known cerebral vascular diseases or abnormalities, and no contraindications for MR imaging examinations as determined on the clinically available questionnaire that had to be filled in before the MR examination.

Qualitative Image Quality Analysis

For the qualitative image quality analysis, all volunteer images were analyzed by 3 readers (S.S., board-certified neuroradiologist with 30 years of experience; Á.S., board-certified neuroradiologist with 7 years of experience; T.S., research assistant with 3 years of experience in medical imaging). For statistical analysis, the scores from reader 1 (S.S.) were considered as the representative values due to reader 1 being the most experienced.

All readers independently evaluated MIP and source images and were thereby blinded to the volunteer details and imaging technique.[1,6] All images were transferred to the IntelliSpace portal workstation and displayed to the readers in a random order and with image annotations switched off (blinded read out). First, the readers determined their overall subjective preference and their overall impression of the VS. Second, they gave their overall impression of the number of vessels visible on coronal and sagittal images. Third, the readers continued with rating the visualization of the following anatomical vessel segments: middle cerebral artery M1, M2–M3, M4 segments, ICA C7 segment, ICA horizontal petrous segment, ICA vertical petrous segment, anterior cerebral artery A1, A2–A3 segments, ACA, posterior communicating artery (PcomA), and ophthalmic artery. Lastly, inhomogeneous intraluminal signal (ie, signal decrease within middle of vessel lumen) within the segments ICA C7, M1, and A1 was evaluated. The 4 sequences (CS 3.5, spiral, spiral 0.8, spiral 0.6) were always compared against the SENSE sequence (criterion standard)[6] using a 5-point Likert scale (1 = much worse, 2 = worse, 3 = similar, 4 = better, 5 = much better). After the rating process, the readers were also questioned about the occurrence of specific artifacts and about the rating process in general. Representative image examples are shown in Figure 3, Figure 4, and Figure 5.

Quantitative Image Quality Analysis

Quantitative measurements were performed by 2 readers (M.W. with 20 years of experience in medical imaging, L.VS. with 7 years of experience in medical imaging) for each volunteer and each sequence, and the average value of both readers was subsequently considered as the representative value for statistical analysis.

Contrast-to-Noise Ratio

For both CNR and CR analysis, 2 circular regions of interest (ROIs) were drawn on source images[1] on the independent workstation IntelliSpace Portal version 10 (Philips Healthcare, Best, the Netherlands). One ROI (size 3.54 ± 0.09 mm^2) was drawn on the basilar artery (ROI_{vessel}) and a second ROI (size 107.85 ± 7.45 mm^2) within the brainstem on the same slice location ($ROI_{brainstem}$). Regions of interest were copied from one sequence to another to ensure equal ROI sizes between the sequences from each volunteer. As shown in Figure 6, a section was chosen, which was at mid feet-head distance of the basilar artery (thus directly below the carotid siphon in the C3 segment). Contrast-to-noise ratio values were derived as:

$$CNR = \frac{mean\ (SI_{ROI_{vessel}})}{SD\ (SI_{ROI_{brainstem}})}$$

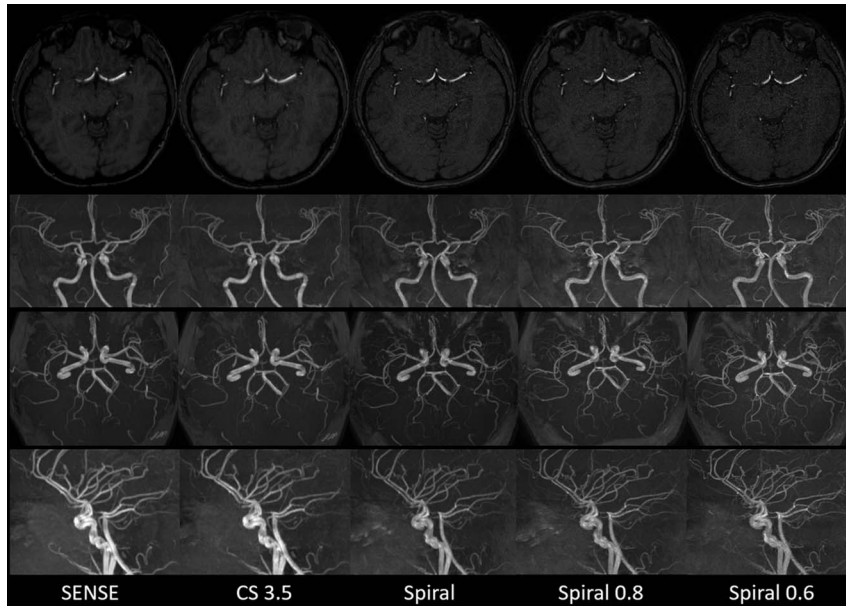

FIGURE 3. Representative examples of source images and maximum intensity projections (MIPs) of the 5 TOF sequences. The decreased CNR of the 3 spiral-TOFs can be observed on the source images.

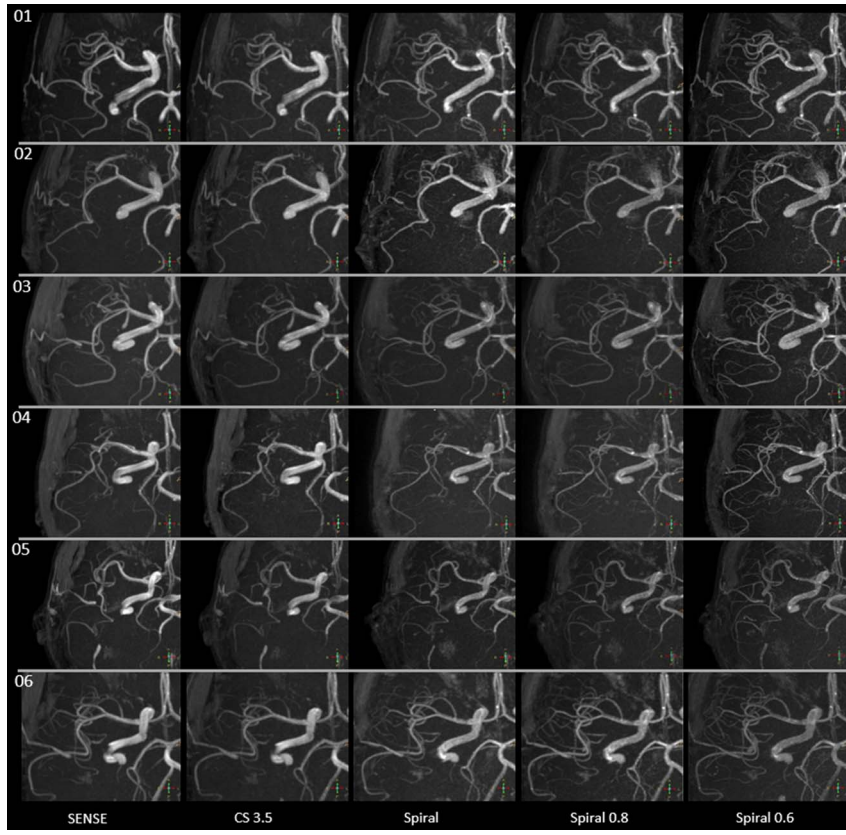

FIGURE 4. Representative examples of maximum intensity projections (MIPs) of the 5 TOF sequences from 6 volunteers.

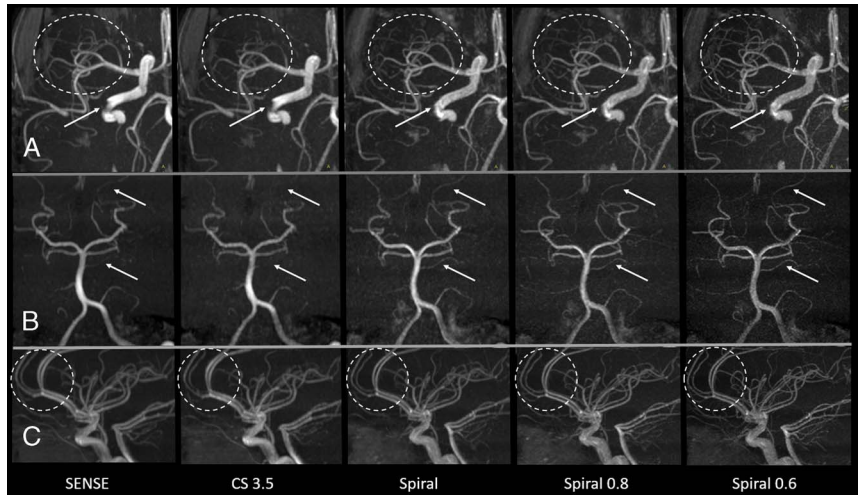

FIGURE 5. Zoomed-in areas of maximum intensity projections (MIPs) of the TOF images from one volunteer. Note the improved vessel visibility and sharpness seen on spiral-TOF images (dashed circles and white arrows in B). Furthermore, an improved visualization of the carotid siphon can be appreciated on the spiral-TOF images (white arrows in A).

Contrast Ratio

Contrast ratio[22] was calculated from the same ROIs as the ones used for CNR using the following formula:

$$CR = \frac{(mean(SI_{ROI_{vessel}}) - mean\ (SI_{ROI_{brainstem}}))}{(mean(SI_{ROI_{vessel}}) + mean\ (SI_{ROI_{brainstem}}))}$$

Vessel Sharpness

For estimation of VS,[23] a line profile perpendicular to the M1 segment of the right middle cerebral artery was generated using FIJI's[20] "Line Profile" function (Fig. 7). To compare the different sequences, signal intensities were normalized to the peak signal intensity along the profile for each sequence. Then the slope of the regression line for the anterior vessel border ($slope_{rise}$) and the posterior vessel border ($slope_{fall}$) was calculated with Excel's built-in "slope function." The mean of $slope_{rise}$ and the absolute value of $slope_{fall}$ was calculated to report a quantitative number for VS.

$$Vessel\ sharpness = mean\left(slope_{rise} + abs\left(slope_{fall}\right)\right)$$

Full-Width at Half Maximum Edge Criterion

The FWHM edge criterion is a quantitative metric that allows for a reliable and robust estimation of a vessel lumen's edge by defining the boundary at 50% intensity level between maximum (lumen) and minimum (tissue). A vessel lumen can therefore be detected with the full width at half maximum criterion, and vessel parameters such as diameter or cross-sectional area can then be derived accurately.[24,25] To generate FWHM values, the line profile from the M1 segment of the right middle cerebral artery computed with FIJI's "Line Profile" function was used. The length (in millimeter) at the half maximum of the line profile curve was measured thus revealing the FWHM value.

Statistical Analysis

Data were initially checked with Levene test for homogeneity of variance, Q-Q plots, and Shapiro-Wilk test for normality of residuals. To compare cross-sectional area measurements from the in vitro study, the Kruskal-Wallis test was applied as residuals were not normally distributed. Values for CNR were log-transformed to achieve normality of residuals. For log-transformed CNR, CR, VS, and FWHM measurements, analysis of variance (ANOVA) or Welch's ANOVA (for unequal variances) was performed to evaluate whether the means were different between the 5 TOFs. In case of a significant result, post hoc tests (Dunnett's post hoc test or Dunnett's T3 post hoc tests for unequal variances) were performed. For qualitative image quality metrics, exact binomial tests were performed to test the null hypothesis that the probability for better results (ratings: 4/5) was equal to the probability for worse results (ratings: 1/2) in comparison to the SENSE sequence. Krippendorff's alpha was computed to evaluate the interreader agreement for qualitative image quality ratings. The following scale was used to indicate the level of agreement: 0.0–0.20 = poor agreement, 0.21–0.40 = fair agreement, 0.41–0.60 = moderate agreement, 0.61–0.80 = substantial agreement, and 0.81–1.00 = almost perfect agreement.[26] A P value of less than 0.05 was considered significant. All analyses were performed in the R programming language (version 3.3.3) (R Core Team, 2017). The package "multcomp" (Hothorm, Bretz, Westfall, 2008) and "DTK" (Lau, 2013) were used to run post hoc tests. The package "irr" (Gamer, Lemon, Fellows, Singh, 2012) was used to compute Krippendorff's alpha.

RESULTS

In Vitro

A detailed overview is provided in Table 2. In summary, the values for cross-sectional area measurements were not significantly different between the 6 sequences ($P = 0.904$). Furthermore, when only comparing values from the 5 TOF sequences (thus not considering the values from the 3D PDw sequence), values were also not significantly different ($P = 0.966$).

In Vivo

Qualitative Image Quality Analysis

A detailed overview of scores is given in Table 3. In brief, the CS 3.5 performed equally well as the SENSE in every category. The spiral sequence performed equally well as the SENSE except for the visualization of the M1 segment, where the spiral sequence performed significantly worse than the SENSE. However, the spiral sequence significantly outperformed the SENSE in terms of VS, visualization of the ICA horizontal petrous segment, and visualization of the A1 segment. The spiral 0.8 and spiral 0.6 sequences outperformed the SENSE in the categories subjective preference, VS, number of vessels visible in both coronal and sagittal fixed positions, visualization of the segments ICA horizontal petrous, ICA vertical petrous, M2–M3, M4, A1, A2–A3, PcomA, and ophthalmic artery. As for inhomogeneous intraluminal signal

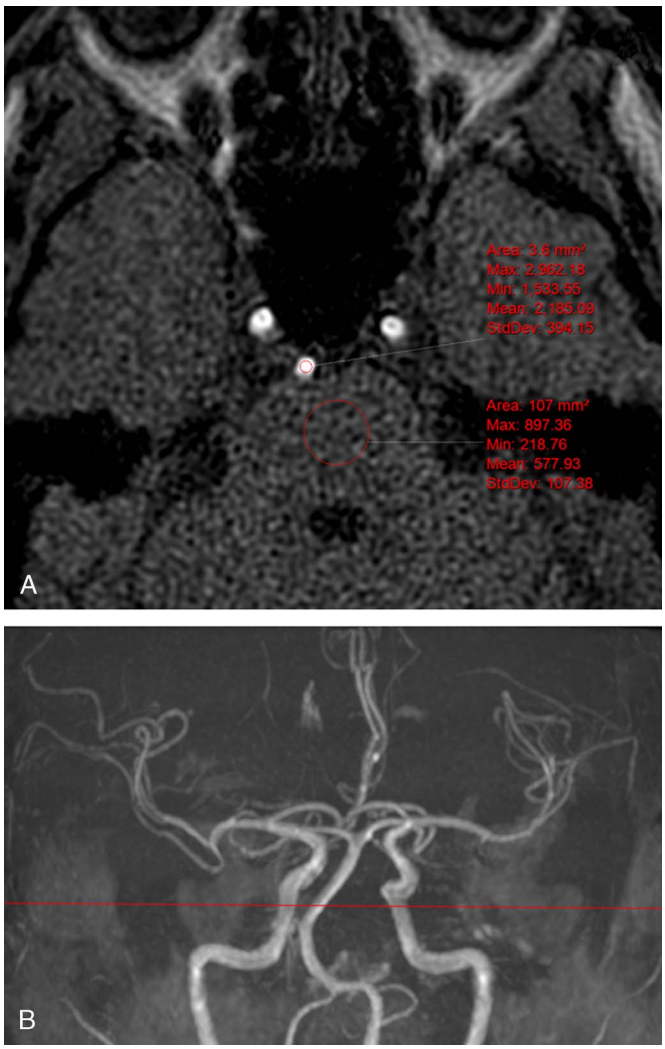

FIGURE 6. Representative example of ROI placement on source images (in this case stemming from the SENSE sequence) for contrast-to-noise ratio (CNR) and contrast ratio (CR) measurements (A). Regions of interest were always placed on a slice as defined by a line that was set directly below the carotid siphon (B).

within the segments ICA C7, M1, and A1, both sequences exhibited significantly worse scores than the SENSE. Lastly, the readers noted that they did not notice any specific artifacts.

Concerning the interreader agreement, poor to substantial agreement was found both when considering all 3 readers and only the 2 most experienced readers. However, on average, interreader agreement was better when only the 2 most experienced readers were considered. In addition, upon questioning, the 3 readers noted that they felt that personal preference played an important role in rating of images. For example, some preferred the visualization of the ICA C7 segment on spiral-TOF images, whereas others preferred the SENSE's or CS 3.5's visualization of the segment. This is reflected in the low interreader agreement in this category.

Quantitative Image Quality Analysis

Detailed results are provided in Table 4 and visualized in Figure 8.

Contrast-to-Noise Ratio

For statistical analysis, the values for CNR were log-transformed to achieve normality of residuals. The ANOVA indicated that the means were different ($P < 0.001$) between the 5 TOFs. Dunnett's post hoc tests showed that the CS 3.5 and all 3 spiral sequences (spiral, spiral 0.8, spiral 0.6) were significantly different from the SENSE. Although the SENSE sequence only slightly outperformed the CS 3.5 in terms of CNR, all 3 spiral sequences presented with considerably lower CNR values than the SENSE. This can even be seen on the grainy and noisy appearing source images of the spiral-TOFs (Fig. 3).

Contrast Ratio

The ANOVA indicated that the group means between the 5 sequences were different ($P = 0.002$). Dunnett's post hoc tests showed that only the spiral sequence differed significantly from the SENSE. Specifically, the spiral sequence slightly exceeded the SENSE's performance in terms of CR.

Vessel Sharpness

Welch's ANOVA and Dunnett's T3 post hoc tests were performed because of unequal variances. Welch's ANOVA indicated that the group means of the 5 sequences were different ($P < 0.001$). Dunnett's T3 post hoc tests showed that there was no significant difference between the CS 3.5 and the SENSE. However, the spiral, spiral 0.8, and spiral 0.6 sequences all significantly outperformed the sense sequence in terms of VS.

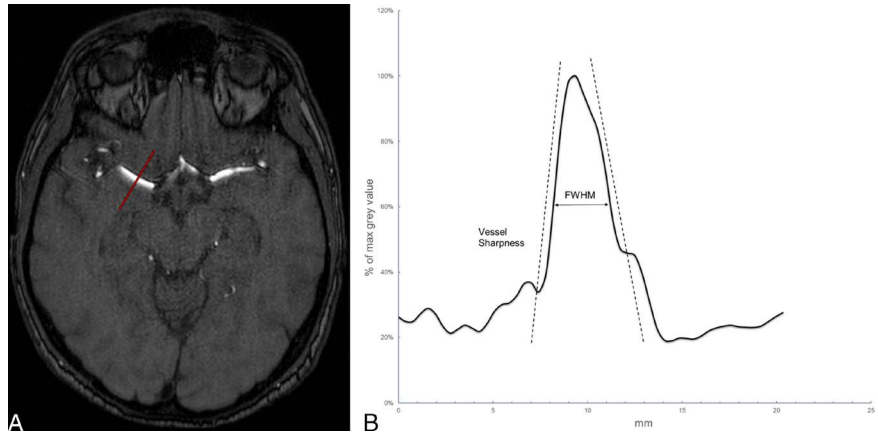

FIGURE 7. Representative example of a TOF source image (A) (in this case stemming from the SENSE sequence) used for quantitative image quality analysis. Based on a line profile perpendicular to the M1 segment of the right middle cerebral artery, vessel sharpness and FWHM values were derived (B).

TABLE 2. Quantitative Data From In Vitro Vessel Tracking Experiments

	3D PDw	SENSE	CS 3.5	Spiral	Spiral 0.8	Spiral 0.6
Area, median [IQR], mm^2	13 [6.5, 22.8]	11.6 [6.4, 15.3]	11.3 [5.7, 14.1]	10.5 [4.4, 14]	10.4 [5.5, 14.9]	10.8 [5.5, 14.1]
Median difference to 3D PDw, mm^2		−0.9	−1.6	−2.0	−1.1	−2.0
Median difference to SENSE, mm^2			−0.3	−1.1	−0.5	−0.8

3D indicates 3-dimensional; PDw, proton density-weighted; IQR, interquartile range.

Full Width at Half Maximum

Although the ANOVA indicated that the group means of the 5 sequences were different ($P = 0.039$), Dunnett's post hoc tests showed that neither the CS 3.5 nor the 3 spiral sequences differed significantly from the SENSE.

DISCUSSION

In this study, we presented data on the first-time use of spiral-TOFs for intracranial vessel imaging at 1.5 T. We tested 5 TOF sequences, of which 3 were spiral-TOFs, one was a CS-accelerated TOF (named CS 3.5), and one was a PI-accelerated TOF (named SENSE). Most importantly, we showed that spiral intracranial vessel imaging was feasible in healthy volunteers as spiral-TOFs (spiral, spiral 0.8, spiral 0.6) outperformed the SENSE in certain qualitative and quantitative image quality metrics. Furthermore, spiral-TOFs may be of interest to clinical institutions as scan times can be reduced considerably beyond what is achievable with currently employed TOFs.

Spiral MR imaging has been described a long time ago[11–15] and has been applied in various settings and anatomies. Specifically, spiral imaging has been used for coronary artery imaging, functional imaging, pelvic imaging, black-blood imaging of peripheral vasculature, and postcontrast brain imaging.[11,15] However, to the best of our knowledge, the spiral acquisition technique has never been utilized in combination with TOF MRA imaging and therein for intracranial vessel imaging.

Parallel imaging–accelerated TOFs such as the SENSE are considered the criterion standard for contrast-free intracranial vessel MR imaging, yet recently, studies comparing CS-accelerated TOFs with PI-accelerated TOFs suggest that CS-accelerated TOFs may be able to replace PI-accelerated TOFs as image quality can be maintained while reducing acquisition times.[1–7]

A recent study has shown that a CS-accelerated TOF achieved comparable image quality as a conventional PI-accelerated TOF. In addition, better delineation of vessel segments, fewer artifacts, and higher CRs were observed when using the CS-accelerated sequence.[7]

A further study led by Lin et al reached a similar conclusion. In their intraindividual comparison study, 49 patients with suspected intracranial arterial diseases were prospectively scanned with both PI- and CS-accelerated sequences. After rating by 3 radiologists, the CS-accelerated sequence was found to exhibit better image quality with less blur, higher signal-to-noise ratio (SNR) and CNR, and comparable image diagnostic performance of intracranial arteries in comparison with the conventional TOF.[1]

Fushimi et al focused specifically for aneurysm imaging. Time-of-flight imaging was performed in 20 patients with 26 aneurysms. Besides rating the overall visualization, the aneurysm dimensions were measured and compared between PI- and CS-accelerated sequences. The authors found no differences between the 2 sequences both in terms of image quality and dimensions of the aneurysms.[2]

Lastly, CS-accelerated TOFs were also found to be reliable alternatives to conventional PI-accelerated TOFs in the imaging of moyamoya disease and for diagnosing intracranial arterial stenosis.[4–6]

Except for a slightly lower CNR observed in our CS 3.5 sequence, we found no significant difference between our CS 3.5 and SENSE sequences. Thus, we largely confirm the findings of previously published studies. In contrast to us, Lin et al observed higher CNR using their PI-accelerated TOF. This discrepancy may be caused by slight differences in the denoising procedure of CS reconstruction.

TABLE 3. Overview of the Qualitative Image Quality Analysis Rating Scores

	Subjective Preference	Vessel Sharpness	No. Vessels Visible (C)	No. Vessels Visible (S)	Visualization of M1	Visualization of M2–M3	Visualization of M4	Visualization of ICA C7
CS 3.5	3 [3, 3]	3 [3, 3]	3 [3, 3]	3 [3, 3]	3 [3, 3]	3 [3, 3]	3 [3, 3]	3 [3, 3]
Spiral	3 [3, 3]	4 [3.25, 4]; 0.016^+	3 [3, 3.75]	3 [3, 3]	2 [2, 3]; 0.031^-	3 [3, 4]	3 [3, 3]	2.5 [2, 3]
Spiral 0.8	4 [3.25, 4]; 0.016^+	4 [4, 4]; 0.002^+	4 [4, 4]; 0.021^+	4 [4, 4]; 0.002^+	3.5 [3, 4]	4 [4, 4]; 0.004^+	4 [4, 4]; 0.008^+	3 [2, 3]
Spiral 0.6	4 [4, 4]; 0.002^+	4 [4, 4]; 0.002^+	4 [4, 4.75]; 0.002^+	4 [4, 4.75]; 0.002^+	3.5 [3, 4]	4 [4, 4]; 0.004^+	4 [4, 4]; 0.002^+	3 [3, 3]
Interreader agreement (3 readers), Krippendorff's alpha	0.461	0.655	0.717	0.737	0.201	0.264	0.69	−0.013
Interreader agreement (2 most experienced readers), Krippendorff's alpha	0.543	0.737	0.788	0.699	0.201	0.347	0.781	0.0268

Scores are given as median [interquartile range]; *P* value. Only significant *P* values are shown, and significantly better scores in comparison to the SENSE sequence are indicated with a superscript "plus" (+) after the *P* value, while significantly worse scores in comparison to the SENSE sequence are indicated with a superscript "minus" (−) after the *P* value.

ICA indicates internal carotid artery; anterior ACA, communicating artery; PcomA, posterior communicating artery.

Although generally the spiral-TOFs in this study outperformed our SENSE, considerably lower CNR was found in all 3 spiral sequences. Contrast-to-noise ratio decreased with increasing resolution of the spiral sequences, and this could even be seen on the source images that appeared noisy—signal-to-noise ratio scales with total voxel volume and the square root of the acquisition time (t_{acq}). The voxel volume equates to the product of slice thickness, the voxel size (x), and the voxel size (y). Contrast-to-noise ratio reflects the difference in SNR between 2 tissue types (a, b). Contrast-to-noise ratio depends on the overall SNR and can be expressed as: CNR = SNRa − SNRb. The voxel volume of the spiral sequence was identical to the voxel volume of the SENSE and CS 3.5 sequences but exhibited a shorter t_{acq}. Therefore, a lower SNR/CNR can be expected. The voxel volume of the spiral 0.8 and spiral 0.6 sequences was smaller than the voxel volume of the SENSE and CS 3.5 sequences. Thus, the decrease in CNR in those 2 sequences is mainly caused by the lower voxel volume.

Yet given the fact that MIPs are often given preference over source images by radiologists to assess intracranial vessel images, this possible drawback of a lower CNR has to be further studied in the clinical setting. The qualitative image quality rating performed mainly on MIPs demonstrated that all spiral-TOFs were similar with our SENSE, whereby the spiral 0.8 and spiral 0.6 sequences even clearly exceeded the SENSEs performance in several categories. However, considerable variability in scores was observed for the qualitative image quality rating, which is reflected in the interreader agreement values. The interreader agreement was better when only the 2 most experienced readers were considered rather than all 3 readers, which may reveal that the experience of raters influenced the scores. Thus for statistical analysis, the values of the most experienced reader served as the representative values. However, upon questioning of the 3 readers, each noted that they felt that personal preference played an important role in rating of images, and this may have been one of the main factors determining the rating scores.

Concerning the other quantitative metrics one spiral-TOF (spiral) outperformed the SENSE sequence, whereas 2 spiral-TOFs (spiral 0.8 and spiral 0.6) performed equally well in terms of CR. Moreover, all 3 spiral-TOFs clearly demonstrated superior VS in comparison to the SENSE. Especially, the spiral 0.8 and spiral 0.6 sequences revealed greatly improved VS, which may also be owing to the higher resolution of these TOFs.

As for the data gathered from the in vitro tests, no statistical difference between the values of the cross-sectional area measurements of any TOF sequence and the 3D PDw sequence were found. This indicates that the spiral-TOFs and CS 3.5 allow for the accurate depiction of intracranial vessels dimensions in comparison to the SENSE and 3D PDw sequence. This is of substantial clinical importance, namely, when diagnosing the degree of occlusion in arterial stenosis and also for imaging and evaluating aneurysms. The fact that the FWHM values (derived from in vivo imaging rather than in vitro) also did not differ significantly between any TOF sequence further corroborates this finding.

Ultimately, the time savings associated with spiral-TOF imaging must be strongly considered. The spiral-TOF (spiral) with equivalent resolution as the SENSE and CS 3.5 clocked in at 1:32 minutes in contrast to 5:08 and 3:06 images for the other sequences, respectively, thus representing a reduction of 70.12% and 50.54% in scan times. Alternatively, depending on the needs of the patient and radiologist, spiral-TOF imaging can also be performed at higher resolutions without prolonging scan times. The spiral 0.8 sequence with an isotropic resolution of 0.8 mm^3 lasted 2:12 minutes thus rendering a scan time reduction of 57.14% compared with the SENSE and a reduction of 29.03% compared with the CS 3.5. As for the spiral 0.6 sequence with an isotropic resolution of 0.6 mm^3, its scan time (5:22 minutes) is largely comparable to that of our SENSE yet displays a notably higher resolution.

Hence the question remains, "Which spiral-TOF sequence renders the best performance?" Our data suggest that the spiral 0.8 sequence exhibits an optimal scan time-quality ratio for normal arteries. This sequence achieves premium intracranial vessel imaging at slightly over 2 minutes while delivering significantly better image quality than the SENSE, CS 3.5, and spiral-TOF. Furthermore, except for VS, the sequence nearly reaches the performance of the much slower spiral 0.6 sequence therein suggesting that the spiral 0.8 is the overall more suitable candidate for future clinical imaging. However, one should also strongly emphasize the impressive performance of the spiral sequence. With its scan time of 1:32 minutes, this TOF truly deserves to be appraised as ultrafast, and considering the fact that the sequence mostly performed as well or even better than our SENSE and CS 3.5, it may be a tempting future candidate for clinical institutions with a very large patient turnover.

For the future, a combination of compressed sensing[27–33] and PI technology together with spiral acquisition may be very interesting as the advantages of either methods can be combined and scan times may be reduced even further. However, the feasibility of such a combination would have to be investigated first.

Visualization of ICA Horizontal Petrous Segment	Visualization of ICA Vertical Petrous Segment	Visualization of A1	Visualization of A2–A3	Visualization of ACA	Visualization of PcomA	Visualization of Ophthalmic Artery	Inhomogeneous Intraluminal Signal (C7/M1/A1)
3 [3, 3]	3 [3, 3]	3 [3, 3]	3 [3, 3]	3 [3, 3]	3 [3, 3]	3 [3, 3]	3 [3, 3]
4 [3, 4]; 0.031^{+}	3 [3, 3.75]	4 [3, 4]; 0.031^{+}	3 [3, 4]	3 [3, 3.5]	3 [3, 3.75]	4 [3, 4]	2.5 [2, 3]
4 [4, 4]; 0.004^{+}	4 [3, 4]; 0.031^{+}	4 [3.25, 4]; 0.016^{+}	4 [4, 4]; 0.004^{+}	3 [3, 4]	4 [4, 4]; 0.008^{+}	4 [4, 4]; 0.021^{+}	2 [2, 2.75]; 0.016^{-}
4 [4, 5]; 0.002^{+}	4.5 [4, 5]; 0.002^{+}	4 [3.25, 4]; 0.016^{+}	4 [4, 4.75]; 0.004^{+}	3 [3, 3.5]	4 [4, 4]; 0.004^{+}	4 [4, 4]; 0.002^{+}	2 [2, 2]; 0.039^{-}
0.661	0.711	0.413	0.492	0.253	0.512	0.624	0.212
0.657	0.691	0.552	0.719	0.323	0.589	0.724	−0.112

TABLE 4. Data From the Quantitative Image Quality Analysis Is Presented

	SENSE	CS 3.5	Spiral	Spiral 0.8	Spiral 0.6
	Mean ± SD	Mean ± SD (95% CI)	Mean ± SD (95% CI)	Mean ± SD (95% CI)	Mean ± SD (95% CI)
CNR	37.48 ± 7.13	31.14 ± 5.97 (0.708, 0.977)	19.77 ± 1.65 (0.455, 0.628)	16.18 ± 2.14 (0.37, 0.511)	10.37 ± 1.05 (0.238, 0.329)
CR	0.53 ± 0.03	0.51 ± 0.03 (−0.042, 0.016)	0.56 ± 0.03 (0.005, 0.064)	0.55 ± 0.02 (−0.01, 0.049)	0.54 ± 0.02 (−0.017, 0.042)
Vessel sharpness	0.37 ± 0.03	0.37 ± 0.03 (−0.064, 0.056)	0.52 ± 0.07 (0.044, 0.259)	0.53 ± 0.08 (0.047, 0.273)	0.73 ± 0.09 (0.231, 0.478)
FWHM	2.4 ± 0.2	2.49 ± 0.25 (−0.307, 0.482)	2.09 ± 0.27 (−0.704, 0.085)	2.14 ± 0.3 (−0.652, 0.137)	2.11 ± 0.31 (−0.679, 0.111)

The 95% CIs from Dunnett's or Dunnett's T3 post hoc tests are shown. The CIs give an estimate for the difference in means between the values of the 2 sequences being compared. Positive lower confidence limits indicate higher values for tested TOF compared with SENSE; negative upper confidence limits indicate lower values for tested TOF compared with SENSE. In the case of CNR, where values were log-transformed for ANOVA, the CI reveals by which factor the values from the 4 sequences (CS 3.5, spiral, spiral 0.8, spiral 0.6) differ from the values from the SENSE sequence. All upper confidence limits are below 1, thus indicating that all tested TOFs have lower values compared with SENSE.

CI indicates confidence interval; CNR, contrast-to-noise ratio; CR, contrast ratio; FWHM, full width at half maximum.

Lastly our study has some limitations. First, the sample size is fairly small, although in the typical range for pilot studies evaluating and comparing the feasibility and quality of novel sequences.[34–40] Second, the vascular phantom was operated with a pump that generated constant rather than oscillating water flow. This may affect the generalizability of our in vitro results since blood flow in vivo is pulsatile. Especially, one might hypothesize that the lower CNR encountered in the spiral-TOFs may become a problem in patients presenting with stenotic or post stenotic arterial areas with low blood flow. Thus, a future study assessing the clinical feasibility of spiral-TOF imaging is of great interest. Third, for comparison reasons, we used a 3D PDw sequence in the in vitro experiments rather than the true dimensions of the phantoms vessels' (which were not known). Lastly, it should be acknowledged that there are many formulas to determine CNR and CR[1]; therefore, results may differ when applying different formulas.

To conclude, we provide data on the performance of 3 spiral-TOFs and a CS-accelerated TOF (named CS 3.5) in comparison to a conventional PI-accelerated TOF (named SENSE) and show that spiral-TOFs deliver high-quality intracranial vessel imaging at unprecedented scan times below 2 minutes. Future clinical studies assessing the diagnostic

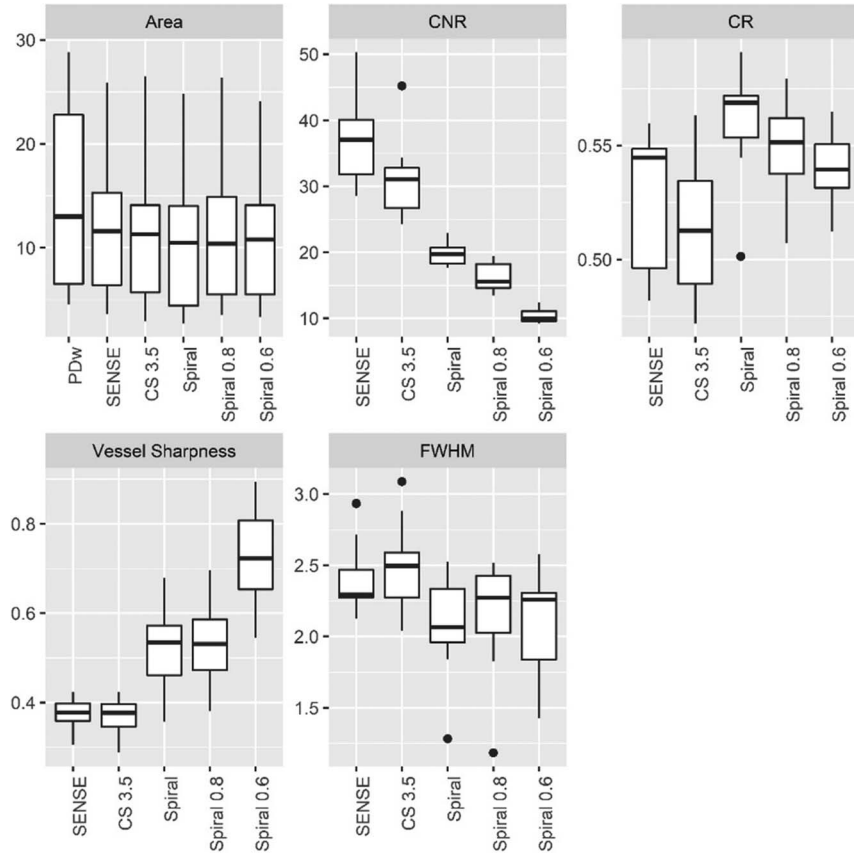

FIGURE 8. Boxplots depicting data from quantitative image quality analysis (in vitro and in vivo). The line in the box shows the median, the lower, and upper hinges correspond to the first and third quartiles. The upper/lower whisker extends from the hinge to the largest/smallest value no further than 1.5 × IQR from the hinge.

accuracy of spiral-TOFs are warranted. Furthermore, an investigation into the use of spiral-TOFs at higher field strengths than 1.5 T would also be of clinical interest.

REFERENCES

1. Lin Z, Zhang X, Guo L, et al. Clinical feasibility study of 3D intracranial magnetic resonance angiography using compressed sensing. *J Magn Reson Imaging*. 2019. doi:10.1002/jmri.26752.
2. Fushimi Y, Okada T, Kikuchi T, et al. Clinical evaluation of time-of-flight MR angiography with sparse undersampling and iterative reconstruction for cerebral aneurysms. *NMR Biomed*. 2017;30. doi:10.1002/nbm.3774.
3. Fushimi Y, Fujimoto K, Okada T, et al. Compressed sensing 3-dimensional time-of-flight magnetic resonance angiography for cerebral aneurysms: optimization and evaluation. *Invest Radiol*. 2016;51:228–235.
4. Lu SS, Qi M, Zhang X, et al. Clinical evaluation of highly accelerated compressed sensing time-of-flight MR angiography for intracranial arterial stenosis. *AJNR Am J Neuroradiol*. 2018;39:1833–1838.
5. Yamamoto T, Okada T, Fushimi Y, et al. Magnetic resonance angiography with compressed sensing: an evaluation of moyamoya disease. *PLoS One*. 2018;13:e0189493.
6. Yamamoto T, Fujimoto K, Okada T, et al. Time-of-flight magnetic resonance angiography with sparse undersampling and iterative reconstruction: comparison with conventional parallel imaging for accelerated imaging. *Invest Radiol*. 2016; 51:372–378.
7. Tang H, Hu N, Yuan Y, et al. Accelerated time-of-flight magnetic resonance angiography with sparse undersampling and iterative reconstruction for the evaluation of intracranial arteries. *Korean J Radiol*. 2019;20:265–274.
8. Sodickson DK, Manning WJ. Simultaneous acquisition of spatial harmonics (SMASH): fast imaging with radiofrequency coil arrays. *Magn Reson Med*. 1997;38:591–603.
9. Griswold MA, Jakob PM, Heidemann RM, et al. Generalized autocalibrating partially parallel acquisitions (GRAPPA). *Magn Reson Med*. 2002;47:1202–1210.
10. Pruessmann KP, Weiger M, Scheidegger MB, et al. SENSE: sensitivity encoding for fast MRI. *Magn Reson Med*. 1999;42:952–962.
11. Li Z, Hu HH, Miller JH, et al. A spiral spin-echo MR imaging technique for improved flow artifact suppression in T1-weighted postcontrast brain imaging: a comparison with Cartesian turbo spin-echo. *AJNR Am J Neuroradiol*. 2016; 37:642–647.
12. Nishimura DG, Irarrazabal P, Meyer CH. A velocity k-space analysis of flow effects in echo-planar and spiral imaging. *Magn Reson Med*. 1995;33:549–556.
13. Yacoe ME, Li KC, Cheung L, et al. Spiral spin-echo magnetic resonance imaging of the pelvis with spectrally and spatially selective radiofrequency excitation: comparison with fat-saturated fast spin-echo imaging. *Can Assoc Radiol J*. 1997;48:247–251.
14. Brewer KD, Rioux JA, D'Arcy RC, et al. Asymmetric spin-echo (ASE) spiral improves BOLD fMRI in inhomogeneous regions. *NMR Biomed*. 2009;22:654–662.
15. Börnert P, Stuber M, Botnar RM, et al. Direct comparison of 3D spiral vs. Cartesian gradient-echo coronary magnetic resonance angiography. *Magn Reson Med*. 2001; 46:789–794.
16. Augsburger L, Reymond P, Fonck E, et al. Methodologies to assess blood flow in cerebral aneurysms: current state of research and perspectives. *J Neuroradiol*. 2009;36:270–277.
17. Hollnagel DI, Summers PE, Kollias SS, et al. Laser Doppler velocimetry (LDV) and 3D phase-contrast magnetic resonance angiography (PC-MRA) velocity measurements: validation in an anatomically accurate cerebral artery aneurysm model with steady flow. *J Magn Reson Imaging*. 2007;26:1493–1505.
18. Sartoretti T, Sartoretti E, Wyss M, et al. Compressed SENSE accelerated 3D T1w black blood turbo spin echo versus 2D T1w turbo spin echo sequence in pituitary magnetic resonance imaging. *Eur J Radiol*. 2019;120:108667.
19. Sartoretti E, Sartoretti T, Binkert C, et al. Reduction of procedure times in routine clinical practice with compressed SENSE magnetic resonance imaging technique. *PLoS One*. 2019;14:e0214887.
20. Sartoretti T, Reischauer C, Sartoretti E, et al. Common artefacts encountered on images acquired with combined compressed sensing and SENSE. *Insights Imaging*. 2018;9:1107–1115.
21. Wang Q, Robson MD, Francis JM, et al. Accuracy of quantitative MR vessel wall imaging applying a semi-automated gradient detection algorithm—a validation study. *J Cardiovasc Magn Reson*. 2004;6:895–907.
22. Fischer A, Kraff O, Maderwald S, et al. Non-enhanced T1-weighted liver vessel imaging at 7 Tesla. *PLoS One*. 2014;9:e97465.
23. Lohöfer FK, Kaissis GA, Rasper M, et al. Magnetic resonance cholangiopancreatography at 3 Tesla: image quality comparison between 3D compressed sensing and 2D single-shot acquisitions. *Eur J Radiol*. 2019;115:53–58.
24. Merkx MA, Bescós JO, Geerts L, et al. Accuracy and precision of vessel area assessment: manual versus automatic lumen delineation based on full-width at half-maximum. *J Magn Reson Imaging*. 2012;36:1186–1193.
25. Ikemura A, Yuki I, Suzuki H, et al. Time-resolved magnetic resonance angiography (TR-MRA) for the evaluation of post coiling aneurysms; a quantitative analysis of the residual aneurysm using full-width at half-maximum (FWHM) value. *PLoS One*. 2018;13:e0203615.
26. Vos EK, Lagemaat MW, Barentsz JO, et al. Image quality and cancer visibility of T2-weighted magnetic resonance imaging of the prostate at 7 tesla. *Eur Radiol*. 2014;24:1950–1958.
27. Eichinger P, Hock A, Schön S, et al. Acceleration of double inversion recovery sequences in multiple sclerosis with compressed sensing. *Invest Radiol*. 2019; 54:319–324.
28. Jungmann PM, Bensler S, Zingg P, et al. Improved visualization of juxtaprosthetic tissue using metal artifact reduction magnetic resonance imaging: experimental and clinical optimization of compressed sensing SEMAC. *Invest Radiol*. 2019; 54:23–31.
29. Yuhasz M, Hoch MJ, Hagiwara M, et al. Accelerated internal auditory canal screening magnetic resonance imaging protocol with compressed sensing 3-dimensional T2-weighted sequence. *Invest Radiol*. 2018;53:742–747.
30. Taron J, Weiss J, Notohamiprodjo M, et al. Acceleration of magnetic resonance cholangiopancreatography using compressed sensing at 1.5 and 3 T: a clinical feasibility study. *Invest Radiol*. 2018;53:681–688.
31. Hausmann D, Niemann T, Kreul D, et al. Free-breathing dynamic contrast-enhanced imaging of the upper abdomen using a Cartesian compressed-sensing sequence with hard-gated and motion-state-resolved reconstruction. *Invest Radiol*. 2019;54:728–736.
32. Yoon JK, Kim MJ, Lee S. Compressed sensing and parallel imaging for double hepatic arterial phase acquisition in gadoxetate-enhanced dynamic liver magnetic resonance imaging. *Invest Radiol*. 2019;54:374–382.
33. Zhu L, Wu X, Sun Z, et al. Compressed-sensing accelerated 3-dimensional magnetic resonance cholangiopancreatography: application in suspected pancreatic diseases. *Invest Radiol*. 2018;53:150–157.
34. Wyss M, Manoliu A, Marcon M, et al. Clinical magnetic resonance imaging of the knee at 7 T: optimization of fat suppression. *Invest Radiol*. 2019;54:160–168.
35. Giraudo C, Motyka S, Weber M, et al. Diffusion tensor imaging of healthy skeletal muscles: a comparison between 7 T and 3 T. *Invest Radiol*. 2019;54:48–54.
36. Stevens KJ, Busse RF, Han E, et al. Ankle: isotropic MR imaging with 3D-FSE-cube—initial experience in healthy volunteers. *Radiology*. 2008;249:1026–1033.
37. Ho MJ, Manoliu A, Kuhn FP, et al. Evaluation of reproducibility of diffusion tensor imaging in the brachial plexus at 3.0 T. *Invest Radiol*. 2017;52:482–487.
38. Stevens KJ, Wallace CG, Chen W, et al. Imaging of the wrist at 1.5 tesla using isotropic three-dimensional fast spin echo cube. *J Magn Reson Imaging*. 2011; 33:908–915.
39. McMahon CJ, Madhuranthakam AJ, Wu JS, et al. High-resolution proton density weighted three-dimensional fast spin echo (3D-FSE) of the knee with IDEAL at 1.5 Tesla: comparison with 3D-FSE and 2D-FSE—initial experience. *J Magn Reson Imaging*. 2012;35:361–369.
40. Stocker D, Manoliu A, Becker AS, et al. Image quality and geometric distortion of modern diffusion-weighted imaging sequences in magnetic resonance imaging of the prostate. *Invest Radiol*. 2018;53:200–206.